NUCL SCI TECH (2022) 33:52
https://doi.org/10.1007/s41365-022-01040-y

Density fluctuations in intermediate-energy heavy-ion collisions

Cong Liu[1,2] · Xian-Gai Deng[3,4] · Yu-Gang Ma[3,4]

Received: 29 March 2022 / Revised: 18 April 2022 / Accepted: 23 April 2022 / Published online: 15 June 2022

Abstract Within the framework of the isospin-dependent quantum molecular dynamics model, we simulate ^{129}Xe + ^{119}Sn collisions in an incident energy range of 20 to 190 MeV/nucleon and discuss the liquid-gas phase transition with density fluctuations. For comparison, we also extract the effective Fisher parameter τ_{eff}, multiplicity of intermediate-mass fragments (IMFs), and information entropy. It is found that the Fisher parameter and maximum information entropy of collisions have peak values at $E_{\mathrm{beam}} = 50$–80 MeV/nucleon. In addition, the maximum multiplicity of IMFs has a plateau around 70 MeV/nucleon. For higher-order density moments in a larger central region of $[-5, 5]^3$ fm^3 in the collision system, a maximum plateau also appears as function of beam energy at energies exceeding 70 MeV/nucleon. These observables, which are consistent with each other, indicate a liquid-gas phase transition around 70 MeV/nucleon for the ^{129}Xe + ^{119}Sn system.

Keywords Heavy-ion collisions · Liquid-gas phase transition · IQMD · Density moment · Intermediate mass fragment · Information entropy · Fisher-law parameter

This work was partially supported by the National Natural Science Foundation of China (Nos. 11890714, 11891070, 12075061, and 12147101), Key Research Program of the CAS (No. XDB34000000), China Postdoctoral Science Foundation (No. 2019M661332), Postdoctoral Innovative Talent Program of China (No. BX20200098); Shanghai Natural Science Foundation (No. 20ZR1404100), and Guangdong Major Project of Basic and Applied Basic Research (No. 2020B0301030008).

✉ Xian-Gai Deng
xiangai_deng@fudan.edu.cn

Yu-Gang Ma
mayugang@fudan.edu.cn

1 Shanghai Institute of Applied Physics, Chinese Academy of Sciences, Shanghai 201800, China

2 University of Chinese Academy of Sciences, Beijing 100049, China

3 Key Laboratory of Nuclear Physics and Ion-beam Application (MOE), Institute of Modern Physics, Fudan University, Shanghai 200433, China

4 Shanghai Research Center for Theoretical Nuclear Physics, NSFC and Fudan University, Shanghai 200438, China

1 Introduction

Exploration of the phase change and equation of state (EOS) of nuclear matter during heavy-ion collisions is an important topic in nuclear physics [1–6]. It is also closely related to the nuclear transport properties [7–15], nuclear landscape, and nuclear synthesis [16–23]. In the late twentieth century, the relationship between the temperature and excitation energy of the system was found to exhibit behavior similar to the macroscopic phenomenon of the liquid-gas phase transition (LGPT) of classical fluid, and it was proposed that a first-order LGPT, and even a second-order phase transition at the critical point, occur in nuclear matter [24]. One expects that in a finite-size system of heavy-ion collisions, the LGPT could appear. The LGPT has been investigated in intermediate-energy heavy-ion collisions, both theoretically and experimentally [25–34]. In recent decades, many probes have been proposed for determining whether the LGPT has occurred, for example, the caloric curve [25–28], intermediate-mass fragments (IMFs) [35, 36], Fisher's power-law exponent of the fragment distribution [35–39], the charge fluctuation of the largest fragment [27, 40–42], the negative heat capacity [43], the information entropy [44–46], and the nuclear Zipf law of Ma [44, 47, 48].

Furthermore, recent research has focused on density fluctuations with the goal of investigating the phase transition theoretically and experimentally as in Refs. [49–51]. The normalized (net) baryon density moments, which are related to the relative production yield of composite baryons, are observationally relevant and may be useful for exploring phase transitions by enhanced production of composite particles [49–53]. The density moment is expected to be an alternative way of identifying the phase transition in heavy-ion collisions.

Because density fluctuations could be associated with the LGPT, the density moments are calculated to investigate the energy dependence and identify the transition. In this study, we explore the dependence of the density moments on the incident energy in intermediate-energy heavy-ion collisions. Within the framework of the isospin-dependent quantum molecular dynamics (IQMD) model, central ^{129}Xe + ^{119}Sn nuclear collisions are simulated, and the density moments are calculated. For verification, the power-law fits of the charge distribution of fragments, fragment multiplicities, and information entropy are presented.

This paper is organized as follows. In Sect. 2, the IQMD model is introduced briefly, and some formulas are presented. In Sect. 3, different LGPT probes are calculated, the maximum values of the density moments are extracted, and the results are discussed. In Sect. 4, a conclusion is presented.

2 Model and formalism

2.1 IQMD model

The QMD model is essentially a quantum extension of the classical molecular dynamics approach, which is widely applied in chemistry and astrophysics; it is designed to describe fragment formation [54–58]. This n-body approach uses a microscopic framework that treats the dynamics of colliding nuclei directly and simulates heavy-ion collisions on an event-by-event basis [54]. The descriptions of mean positions and momenta are purely classical, and particles are considered to be distinguishable in the QMD model [55]. In this work, we use an improved version of the QMD model that incorporates isospin-dependent interactions and the Pauli exclusion principle. In this model, each nucleon is treated as a Gaussian wave packet in a coherent state [54, 55, 59]:

$$\phi_i(\vec{r},t) = \frac{1}{(2\pi L)^{3/4}} \exp\left[-\frac{(\vec{r}-\vec{r}_i(t))^2}{4L} + \frac{\mathbf{i}\vec{p}_i(t)\cdot\vec{r}}{\hbar}\right], \qquad (1)$$

where $\vec{r}_i$ and $\vec{p}_i$ represent the position and momentum of the i-th nucleon, respectively. L is the square of the Gaussian wave packet width, which is set to 2.16 fm^2. The following interaction terms are included in the IQMD model:

$$V_{\rm tot} = V_{\rm sky} + V_{\rm yuk} + V_{\rm sym} + V_{\rm MDI} + V_{\rm Coul}; \qquad (2)$$

they correspond to Skyrme, Yukawa, symmetry, momentum-dependent, and Coulomb interactions, respectively. The detailed forms of these interaction terms are given in Refs. [54, 55]. The Skyrme potential component of the EOS, which is associated with the Skyrme interaction, is given by

$$U_{\rm sky} = \alpha\frac{\rho}{\rho_0} + \beta\left(\frac{\rho}{\rho_0}\right)^{\gamma}. \qquad (3)$$

In this work, we set $\alpha = -129$ MeV, $\beta = 59$ MeV, and $\gamma = 2.09$, which is called the hard EOS, and $\alpha = -390$ MeV, $\beta = 320$ MeV, and $\gamma = 1.14$, which is called the soft EOS.

2.2 Formulas

The following probes are calculated on the basis of information on the phase space and fragments: the Fisher parameter $\tau_{\rm eff}$, fragment multiplicity, information entropy (H), and density moments. The effective Fisher parameter $\tau_{\rm eff}$ can be obtained from the charge distribution by power-law fitting as follows:

$$\mathrm{d}N/\mathrm{d}Z \sim Z^{-\tau_{\rm eff}}. \qquad (4)$$

Here, the charge distribution is taken at 300 fm/c when the system has reached the kinetic freeze-out stage. These charge distributions can be fitted well in the range $3 \leqslant Z \leqslant 7$, as shown in Fig. 1. The charge range is selected to avoid the lightest fragments, with $Z = 1$ and 2, which could be affected by the evaporation and decay process, as well as heavier residual fragments.

The information entropy H of all multiplicity events, which was presented for the first time by Ma [44] and introduced into the study of LGPTs of nuclei, is given by

$$H = -\sum_i f_i \ln f_i, \qquad (5)$$

where f_i, which is calculated for the event space, is the normalized event probability that i particles are produced, and $\sum_i f_i = 1$. The sum is taken over the entire distribution of f_i [44].

The density moments can be calculated from the phase space data computed in an IQMD simulation. First, from

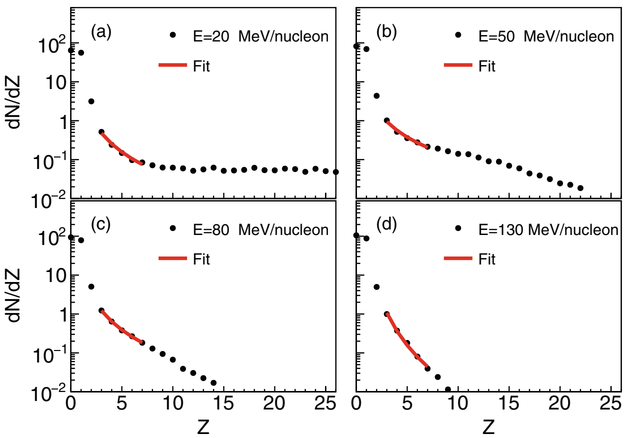

Fig. 1 (Color online) Charge distributions of the systems in freeze-out stage ($t = 300$ fm/c) at beam energies of E of **a** 20 MeV/nucleon, **b** 50 MeV/nucleon, **c** 80 MeV/nucleon, and **d** 130 MeV/nucleon. The red lines represent the Fisher power-law fits in the charge range $3 \leqslant Z \leqslant 7$ for the hard EOS

the phase space data computed by the IQMD simulation, the nuclear matter densities can be calculated at each coordinate space point and at every time as follows:

$$\rho(\vec{r}, t) = \sum_{i=1}^{A_T+A_P} \frac{1}{(2\pi L)^{3/2}} \exp\left[\frac{-(\vec{r} - \vec{r}_i)^2}{2L}\right], \tag{6}$$

where the summation is taken over all nucleons. Then, the numerical value of the nuclear matter density can be used to calculate the density moments via the formula described in Refs. [49–51], that is,

$$\langle \rho^N \rangle \equiv \frac{1}{A} \int \rho(\vec{r})^N \rho(\vec{r}) \mathrm{d}^3 r, \tag{7}$$

where $A = \int \rho(\vec{r}) \mathrm{d}^3 r$. The normalized density moments are given by $\langle \rho^N \rangle / \langle \rho \rangle^N$, which is thus unity for $N = 1$ [49–51]. These quantities have observational relevance because of their intimate relationship with the relative production yield of fragments.

3 Calculations and discussion

Simulations were performed using the IQMD model for central collisions of ^{129}Xe + ^{119}Sn at various beam energies ranging from 20 to 190 MeV/nucleon. Both the hard and soft EOSs were considered. The calculated time range was 0–800 fm/c. The density moments were calculated within central regions consisting of $[-3, 3]^3$ and $[-5, 5]^3$ fm^3 cubic boxes, whose centers are located at the center of mass of the collision system, to check the central area dependence of the observables.

3.1 Time evolution of properties

Figure 2 shows the time evolution of the IMF multiplicity (N_{IMF}) and information entropy (H) at various incident energies. In Fig. 2a, the IMF multiplicity increases, reaches a maximum, and then decreases with increasing time. Here, IMFs are defined as fragments with charge number (Z) greater than or equal to 3 and smaller than the charge number of the source. As the energy increases, the IMF multiplicity changes more rapidly. Thus, at higher energies, the collision system generally has a higher excitation energy and breaks more rapidly into numerous fragments.

Using the distribution $\{f_i\}$ calculated from all events, one can obtain the information entropy (H), as shown in Fig. 2b. The pattern of H evolution is slightly different from that of the IMF multiplicity. With increasing H, the system becomes more chaotic. In the compression stage, the information entropy increases rapidly. With increasing time, more fragments are created, and the multiplicity probability distribution f_i becomes more diverse. As time increases further, the information entropy decreases slightly because long-term binding of nucleons in clusters is difficult under the IQMD Hamiltonian. Thus, the number of particles produced will increase with time, which will result in a change in the probability distribution f_i and finally a slight decrease in H.

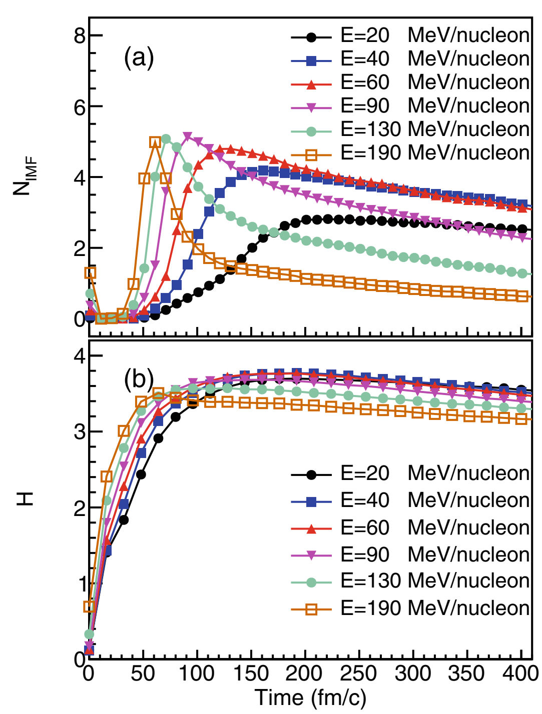

Fig. 2 (Color online) Time evolution of **a** IMF multiplicity and **b** information entropy at different beam energies for the hard EOS

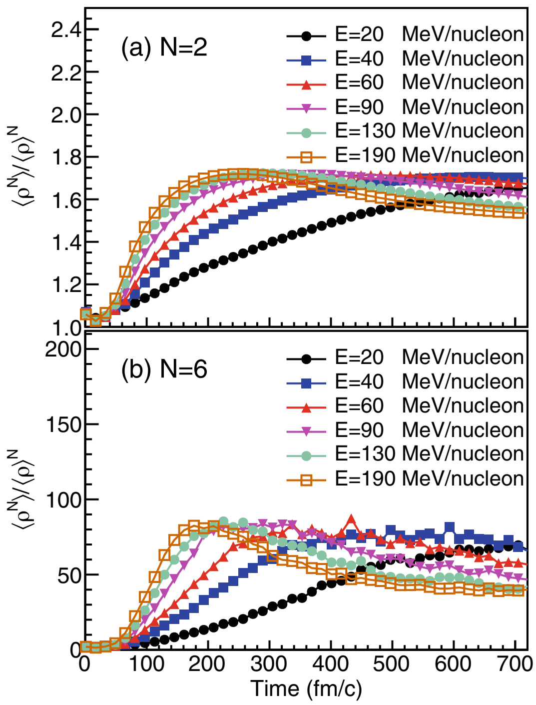

Fig. 3 (Color online) Time evolution of **a** normalized density moments for the orders $N = 2$ and **b** $N = 6$ at different beam energies. Here, the normalized density moments are calculated for the central region of $[-3, 3]^3$ fm^3 for the hard EOS

Figure 3 shows the time evolution of the normalized density moments ($\langle\rho^N\rangle/\langle\rho\rangle^N$), which is the major focus of this work, in the central region of $[-3, 3]^3$ fm^3 at various incident energies for $N = 2$ and 6. The time evolution of the normalized density moments is similar to that of the IMF multiplicity. It increases with time and then shows near-saturation or a slight decrease. At a given energy, for higher-order density moments, the density moment values are larger. In particular, high-order moments show cleaner structure as a function of beam energy, that is, a clearer broad peak structure at a certain energy, although there are larger fluctuations, as shown in Fig. 3b, because obtaining higher-order density moments with the same precision requires better statistics. In addition, higher-order density moments are more sensitive to density fluctuations.

3.2 Discussion of liquid-gas phase transition

To discuss the LGPT in collisions, we extracted the effective Fisher parameter τ_{eff} (Fig. 1), maximum IMF multiplicity (Fig. 2a), and maximum information entropy (Fig. 2b) as a function of incident energy, as shown in Fig. 4. Both τ_{eff} and the maximum information entropy exhibit non-monotonic behavior, and the peak values are approximately 50–80 MeV/nucleon. For the maximum IMF multiplicity, a plateau appears at energies above

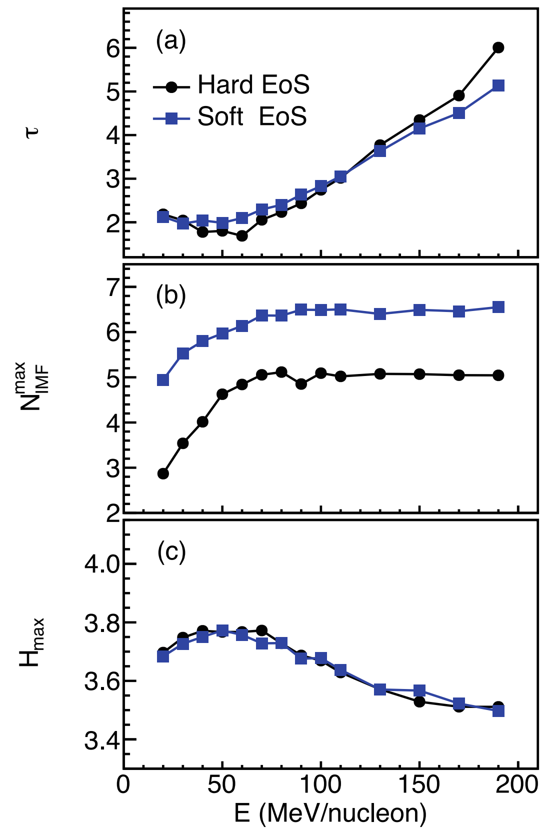

Fig. 4 Extracted values of **a** effective Fisher parameter (τ), **b** maximum values of IMF multiplicities ($N_{\mathrm{IMF}}^{\max}$), and **c** maximum values of information entropy ($H_{\max}$) as a function of incident energy for the hard and soft EOSs

70 MeV/nucleon. All of these results seem consistent with each other, and they indicate that the LGPT for this system could occur in this energy region. The hard and soft EOSs are indicated by black lines with circles and blue lines with squares, respectively, in Fig. 4. The turning energies are not sensitive to the EOS for all τ_{eff}, $N_{\mathrm{IMF}}^{\max}$, and $H_{\max}$. In addition, only the value of $N_{\mathrm{IMF}}^{\max}$ is higher for the soft EOS than for the hard EOS, as shown in Fig. 4b. We also deduced the temperature using the fluctuation in the proton transverse momentum [60], which is defined as $\sigma^2 = \langle Q_{xy}^2\rangle - \langle Q_{xy}\rangle^2 = 4m^2T^2$, where $Q_{xy} = p_x^2 - p_y^2$. When temperature is used as a variable instead of incident energy, as shown in Fig. 5, the turning temperature is shifted to slightly lower temperature for all τ_{eff}, $N_{\mathrm{IMF}}^{\max}$, and $H_{\max}$ for the soft EOS. Thus, the soft EOS can reduce the phase transition temperature of a collision system.

Further, we give the maximum normalized density moments for different orders, as shown in Fig. 6. To present all the orders of the normalized density moment in a single figure, these lines are scaled by different factors. In addition, because statistical fluctuations exist, these lines are fitted by polynomial functions. For the order $N = 2$

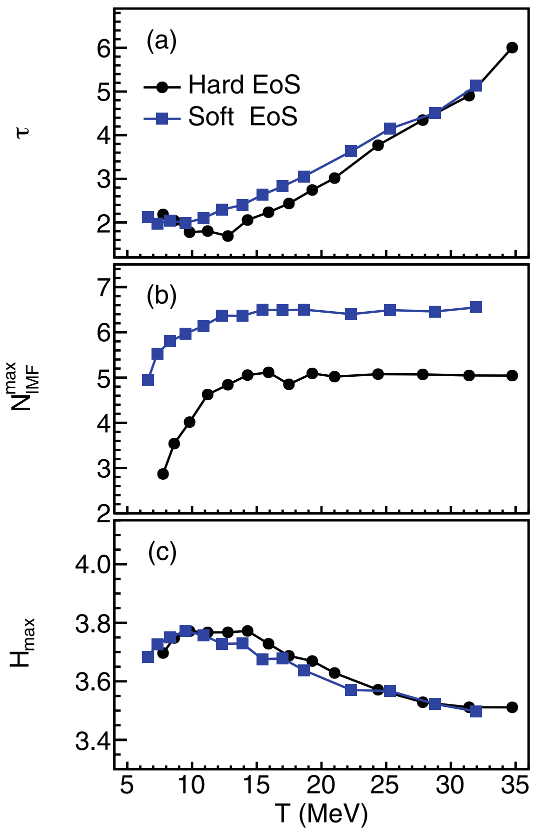

Fig. 5 Same as Fig. 4 but as a function of temperature

(black dotted line in Fig. 6a), the line seems flat. As the order of the density moment increases to $N = 6$, the maximum values appear around $E = 90$ MeV/nucleon, as shown in Fig. 6b. Thus, the collision system has the maximum density fluctuation around $E = 90$ MeV/nucleon, indicating that the LGPT could occur here when the system enters spinodal instability [53, 61]. However, if we choose a larger central region of $[-5, 5]^3$ fm^3, as shown in Fig. 7, the maximum normalized density moments reach maximum values around 70 MeV/nucleon and have a plateau at higher incident energies, like the maximum IMF multiplicity shown in Fig. 4b. This energy is also close to the energy given by the effective Fisher parameter τ and the maximum information entropy, as shown in Fig. 4a and 4c.

Note that the turning energy varies with the central region. That is, the turning point has regional dependence. In fact, this can be understood from the central densities of the selected regions. We found that the $[-3, 3]^3$ fm^3 region can reach a higher average density than the $[-5, 5]^3$ fm^3 region. Thermodynamically, the temperature, pressure, and density are correlated; therefore, the turning point of the energy depends on the density. Actually, as reported in our previous work [62], the temperature extracted from heavy-ion collisions is lower for a smaller central region, where a

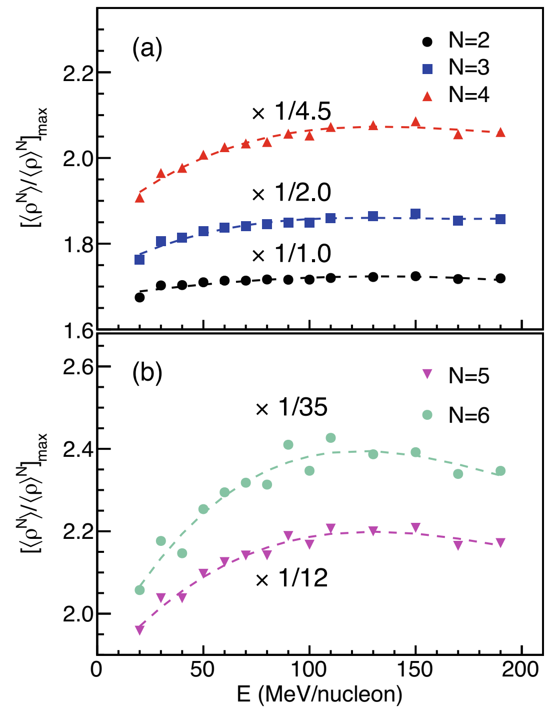

Fig. 6 (Color online) Maximum values of normalized density moments for N = 2, 3, 4, 5, and 6 as a function of incident energy in central region of $[-3, 3]^3$ fm^3. The lines are the fitted results for the hard EOS

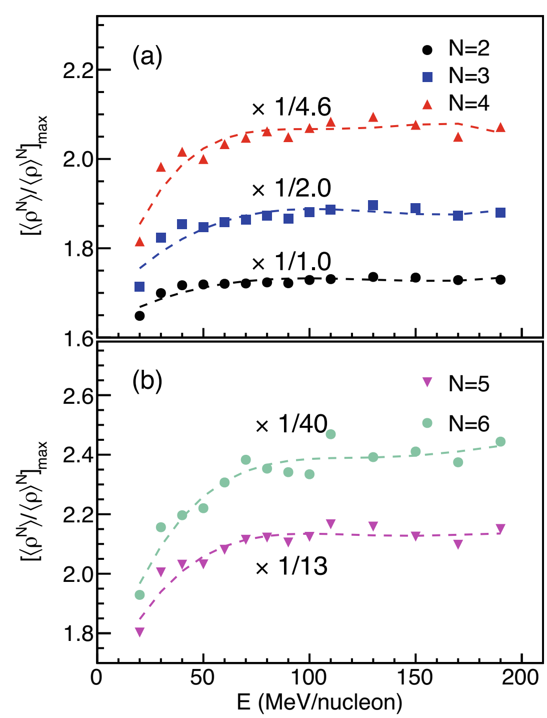

Fig. 7 (Color online) Same as Fig. 6, but for central region of $[-5, 5]^3$ fm^3

higher beam energy would be required to reach the same temperature in a smaller central region. Thus, the calculated density moments for a region of a certain size correspond to a certain density and temperature. The $[-5, 5]^3$ fm^3 is generally a more reasonable option, because our other observables, that is, the fragment distributions and their effective Fisher parameters, the IMF multiplicities, and the information entropy, are those of the entire space.

4 Conclusion

Heavy-ion collisions of ^{129}Xe + ^{119}Sn were simulated by the IQMD model. We calculated the fragment charge distribution, IMF multiplicity, and information entropy. Turning points were found at $E = 50$–80 MeV/nucleon from the effective Fisher parameter τ_{eff} of the fragment charge distribution, maximum IMF multiplicity, and maximum information entropy as a function of incident energy, which are associated with the LGPT. In addition, the turning energy extracted using τ_{eff} seems to be smaller than that obtained using the IMFs. For both the hard and soft EOSs, the turning beam energies from all of the above observables of the phase change are not sensitive to the EOS, but a soft EOS could reduce the phase transition temperature of this collision system. Furthermore, we analyzed the density fluctuations in heavy-ion collisions with density moments of different orders. The obtained turning points are close to those given by effective Fisher parameter, IMF multiplicity, and information entropy. For higher-order normalized density moments, there are also peaks or saturation regions versus beam energy, which have the same properties as those obtained using the IMF multiplicity and information entropy. However, they depend on the size of the region; that is, they are pressure- or density-dependent.

References

1. B. Borderie, J.D. Frankland, Liquid-gas phase transition in nuclei. Prog. Part. Nucl. Phys. **105**, 82–138 (2019). https://doi.org/10.1016/j.ppnp.2018.12.002
2. B.A. Li, L.W. Chen, C.M. Ko, Recent progress and new challenges in isospin physics with heavy-ion reactions. Phys. Rep. **464**, 113–281 (2008). https://doi.org/10.1016/j.physrep.2008.04.005
3. Y.G. Ma, W.Q. Shen, Recent progress of nuclear liquid gas phase transition. Nucl. Sci. Tech. **15**, 4–29 (2004)
4. C.-W. Ma, Y.-G. Ma, Shannon information entropy in heavy-ion collisions. Prog. Part. Nucl. Phys. **99**, 120 (2018). https://doi.org/10.1016/j.ppnp.2018.01.002
5. B. Borderie, M.F. Rivet, Nuclear multifragmentation and phase transition for hot nuclei. Prog. Part. Nucl. Phys. **61**, 551 (2008). https://doi.org/10.1016/j.ppnp.2008.01.003
6. G. Giuliani, H. Zheng, A. Bonasera, The many facets of the (non-relativistic) nuclear equation of state. Prog. Part. Nucl. Phys. **76**, 116 (2014). https://doi.org/10.1016/j.ppnp.2014.01.003
7. P. Danielewicz, Transport properties of excited nuclear matter and the shock-wave profile. Phys. Lett. B **146**, 168 (1984). https://doi.org/10.1016/0370-2693(84)91010-4
8. L. Shi, P. Danielewicz, Nuclear isospin diffusivity. Phys. Rev. C **68**, 064604 (2003). https://doi.org/10.1103/PhysRevC.68.064604
9. R.A. Lacey, N.N. Ajitanand, J.M. Alexander et al., Has the QCD critical point been signaled by observations at the BNL relativistic heavy ion collider? Phys. Rev. Lett. **98**, 092301 (2007). https://doi.org/10.1103/PhysRevLett.98.092301
10. S.X. Li, D.Q. Fang, Y.G. Ma et al., Shear viscosity to entropy density ratio in the Boltzmann–Uehling–Uhlenbeck model. Phys. Rev. C **84**, 024607 (2011). https://doi.org/10.1103/PhysRevC.84.024607
11. C.L. Zhou, Y.G. Ma, D.Q. Fang et al., Thermodynamic properties and shear viscosity over entropy-density ratio of the nuclear fireball in a quantum-molecular dynamics model. Phys. Rev. C **88**, 024604 (2013). https://doi.org/10.1103/PhysRevC.88.024604
12. J. Xu, L.W. Chen, C.M. Ko et al., Shear viscosity of neutron-rich nucleonic matter near its liquid-gas phase transition. Phys. Lett. B **727**, 244 (2013). https://doi.org/10.1016/j.physletb.2013.10.051
13. D.Q. Fang, Y.G. Ma, C.L. Zhou, Shear viscosity of hot nuclear matter by the mean free path method. Phys. Rev. C **89**, 047601 (2014). https://doi.org/10.1103/PhysRevC.89.047601
14. C.Q. Guo, Y.G. Ma, W.B. He et al., Isovector dipole resonance and shear viscosity in low energy heavy-ion collisions. Phys. Rev. C **95**, 054622 (2017). https://doi.org/10.1103/PhysRevC.95.054622
15. X.G. Deng, Y.G. Ma, Y.X. Zhang, Green–Kubo formula for Boltzmann and Fermi–Dirac statistics. Eur. Phys. J. A **57**, 242 (2021). https://doi.org/10.1140/epja/s10050-021-00550-4
16. H.L. Liu, D.D. Han, Y.G. Ma et al., Network structure of thermonuclear reactions in nuclear landscape. Sci. China Phys. Mech. Astron. **63**, 112062 (2020). https://doi.org/10.1007/s11433-020-1552-2
17. H.L. Liu, D.D. Han, P. Ji et al., Reaction rate weighted multilayer nuclear reaction network. Chin. Phys. Lett **37**, 112601 (2020). https://doi.org/10.1088/0256-307X/37/11/112601
18. C.A. Bertulani, Topology of nuclear reaction networks of interest for astrophysics. Sci. China Phys. Mech. Astron. **63**, 112063 (2020). https://doi.org/10.1007/s11433-020-1553-6
19. Y.H. Ge, Y. Zhang, J.N. Hu, Effects of pairing correlation on neutron drop. Sci. China Phys. Mech. Astron. **63**, 242011 (2020). https://doi.org/10.1007/s11433-019-1455-9
20. T.L. Ma, B. Guo, D.Y. Pang et al., New determination of astrophysical 14C(n, γ)15C reaction rate from the spectroscopic factor of ^{15}C. Sci. China Phys. Mech. Astron. **63**, 212021 (2020). https://doi.org/10.1007/s11433-019-9411-2
21. C.J. Jiang, Y. Qiang, D.-W. Guan et al., From finite nuclei to neutron stars: the essential role of high-order density dependence in effective forces. Chin. Phys. Lett **38**, 052101 (2021). https://doi.org/10.1088/0256-307X/38/5/052101
22. J. Xu, Constraining isovector nuclear interactions with giant dipole resonance and neutron skin in ^{208}Pb from a Bayesian approach. Chin. Phys. Lett **38**, 042101 (2021). https://doi.org/10.1088/0256-307X/38/4/042101
23. C.-W. Ma, H.L. Wei, X.Q. Liu et al., Nuclear fragments in projectile fragmentation reactions. Prog. Part. Nucl. Phys **121**, 103911 (2021). https://doi.org/10.1016/j.ppnp.2021.103911

24. J. Pochodzalla, T. Möhlenkamp, T. Rubehn et al. (ALADIN Collaboration), Probing the nuclear liquid-gas phase transition. Phys. Rev. Lett **75**, 1040 (1995). https://doi.org/10.1103/PhysRevLett.75.1040
25. Y.G. Ma, A. Siwek, J. Peter et al. (INDRA Collaboration), Surveying the nuclear caloric curve. Phys. Lett. B **390**, 41 (1997). https://doi.org/10.1016/S0370-2693(96)01372-X
26. J.B. Natowitz, R. Wada, K. Hagel et al., Caloric curves and critical behavior in nuclei. Phys. Rev. C **65**, 034618 (2002). https://doi.org/10.1103/PhysRevC.65.034618
27. Y.G. Ma, J.B. Natowitz, R. Wada et al., Critical behavior in light nuclear systems: experimental aspects. Phys. Rev. C **71**, 054606 (2005). https://doi.org/10.1103/PhysRevC.71.054606
28. A. Rios, Effective interaction dependence of the liquid-gas phase transition in symmetric nuclear matter. Nucl. Phys. A **845**, 58–87 (2010). https://doi.org/10.1016/j.nuclphysa.2010.05.057
29. R. Wang, Y.G. Ma, R. Wada et al., Nuclear liquid-gas phase transition with machine learning. Phys. Rev. Res. **2**, 043202 (2020). https://doi.org/10.1103/PhysRevResearch.2.043202
30. S. Yang, X.D. Sun, J. Geng et al., Liquid-gas phase transition of thermal nuclear matter and the in-medium balance between nuclear attraction and repulsion. Phys. Rev. C **103**, 014304 (2021). https://doi.org/10.1103/PhysRevC.103.014304
31. S.S. Wang, Y.G. Ma, X.G. Cao et al., Hard-photon production and its correlation with intermediate-mass fragments in a framework of a quantum molecular dynamics model. Phys. Rev. C **102**, 024620 (2020). https://doi.org/10.1103/PhysRevC.102.024620
32. O. Savchuk, V. Vovchenko, R.V. Poberezhnyuk et al., Traces of the nuclear liquid-gas phase transition in the analytic properties of hot QCD. Phys. Rev. C **101**, 035205 (2020). https://doi.org/10.1103/PhysRevC.101.035205
33. W. Lin, P. Ren, H. Zheng et al., Solidarity of signal of measures for the liquid-gas phase transition in the statistical multifragmentation model. Phys. Rev. C **99**, 054616 (2019). https://doi.org/10.1103/PhysRevC.99.054616
34. R. Wada, W. Lin, P. Ren et al., Experimental liquid-gas phase transition signals and reaction dynamics. Phys. Rev. C **99**, 024616 (2019). https://doi.org/10.1103/PhysRevC.99.024616
35. M.E. Fisher, The theory of equilibrium critical phenomena. Rep. Prog. Phys. **30**, 615 (1969). https://doi.org/10.1088/0034-4885/30/2/306
36. Y.G. Ma, W.Q. Shen, Onset of multifragmentation in intermediate energy light asymmetrical collisions. Phys. Rev. C **51**, 710 (1995). https://doi.org/10.1103/PhysRevC.51.710
37. M. Huang, R. Wada, Z. Chen et al., Power law behavior of the isotope yield distributions in the multifragmentation regime of heavy ion reactions. Phys. Rev. C **82**, 054602 (2010). https://doi.org/10.1103/PhysRevC.82.054602
38. J.B. Elliott, L.G. Moretto, L. Phair et al., Liquid to vapor phase transition in excited nuclei. Phys. Rev. Lett. **88**, 042701 (2002). https://doi.org/10.1103/PhysRevLett.88.042701
39. Y.G. Ma, R. Wada, K. Hagel et al., Evidence of critical behavior in the disassembly of nuclei with A-36. Phys. Rev. C **69**, 031604 (2004). https://doi.org/10.1103/PhysRevC.69.031604
40. C.O. Dorso, V.C. Latora, A. Bonasera, Signals of critical behavior in fragmenting finite systems. Phys. Rev. C **60**, 034606 (1999). https://doi.org/10.1103/PhysRevC.60.034606
41. B. Borderie, Dynamics and thermodynamics of the liquid-gas phase transition in hot nuclei studied with the INDRA array. J. Phys. GPhys. G **28**, 217 (2002). https://doi.org/10.1088/0954-3899/28/8/201
42. J. Su, L. Zhu, E.X. Xiao, Fluctuations of the largest fragment charge in projectile fragmentation and its nonequilibrium effect. Phys. Rev. C **105**, 024608 (2022). https://doi.org/10.1103/PhysRevC.105.024608
43. Ph. Chomaz, V. Duflot, F. Gulminelli, Caloric curves and energy fluctuations in the microcanonical liquid-gas phase transition. Phys. Rev. Lett. **85**, 3587 (2000). https://doi.org/10.1103/PhysRevLett.85.3587
44. Y.G. Ma, Application of information theory in nuclear liquid gas phase transition. Phys. Rev. Lett. **83**, 3617 (1999). https://doi.org/10.1103/PhysRevLett.83.3617
45. C.W. Ma, Y.P. Liu, H.L. Wei et al., Determination of neutron-skin thickness using configurational information entropy. Nucl. Sci. Tech. **33**, 6 (2022). https://doi.org/10.1007/s41365-022-00997-0
46. F. Li, G. Chen, The evolution of information entropy components in relativistic heavy-ion collisions. Eur. Phys. J. A **56**, 167 (2020). https://doi.org/10.1140/epja/s10050-020-00169-x
47. Y.G. Ma, Zpif's law in the liquid gas phase transition of nuclei. Eur. Phys. J. A **6**, 367 (1999). https://doi.org/10.1007/s100500050355
48. Y.G. Ma, Moment analysis and Zipf law. Eur. Phys. J. A **30**, 227 (2006). https://doi.org/10.1140/epja/i2006-10119-4
49. J. Steinheimer, J. Randrup, Spinodal amplification of density fluctuations in fluid-dynamical simulations of relativistic nuclear collisions. Phys. Rev. Lett. **109**, 212301 (2012). https://doi.org/10.1103/PhysRevLett.109.212301
50. J. Steinheimer, J. Randrup, Spinodal density enhancements in simulations of relativistic nuclear collisions. Phys. Rev. C **87**, 054903 (2013). https://doi.org/10.1103/PhysRevC.87.054903
51. J. Steinheimer, J. Randrup, Spinodal amplification and baryon number fluctuations in nuclear collisions at NICA. Eur. Phys. J. A **52**, 239 (2016). https://doi.org/10.1140/epja/i2016-16239-2
52. X.G. Deng, P. Danielewicz, Y.G. Ma et al., submitted to Phys. Rev. C
53. F. Li, C.M. Ko, Spinodal instabilities of baryon-rich quark matter in heavy ion collisions. Phys. Rev. C **95**, 055203 (2017). https://doi.org/10.1103/PhysRevC.95.055203
54. J. Aichelin, "Quantum'' molecular dynamics—a dynamical microscopic n-body approach to investigate fragment formation and the nuclear equation of state in heavy ion collisions. Phys. Rep. **202**, 233 (1991). https://doi.org/10.1016/0370-1573(91)90094-3
55. Ch. Hartnack et al., Modelling the many-body dynamics of heavy ion collisions: present status and future perspective. Eur. Phys. J. A **1**, 151 (1998). https://doi.org/10.1007/s100500050045
56. C.C. Guo, J. Su, L. Zhu, Secondary decay effects of the isospin fractionation in the projectile fragmentation at GeV/nucleon. Nucl. Sci. Tech. **31**, 123 (2020). https://doi.org/10.1007/s41365-020-00832-4
57. H. Yu, D.Q. Fang, Y.G. Ma, Investigation of the symmetry energy of nuclear matter using isospin-dependent quantum molecular dynamics. Nucl. Sci. Tech. **31**, 61 (2020). https://doi.org/10.1007/s41365-020-00766-x
58. Y.J. He, C.C. Guo, J. Su et al., Study on deuteron formation mechanism in nucleon-induced reactions. Nucl. Sci. Tech. **31**, 84 (2020). https://doi.org/10.1007/s41365-020-00788-5
59. H.L. Liu, Y.G. Ma, A. Bonasera et al., Mean free path and shear viscosity in central ^{129}Xe + ^{119}Sn collisions below 100 MeV/nucleon. Phys. Rev. C **96**, 064604 (2017). https://doi.org/10.1103/PhysRevC.96.064604
60. S. Wuenschel, A. Bonasera, L.W. May et al., Measuring the temperature of hot nuclear fragments. Nucl. Phys. **843**, 1–13 (2010). https://doi.org/10.1016/j.nuclphysa.2010.04.013
61. C.M. Ko, F. Li, Density fluctuations in baryon-rich quark matter. Nucl. Sci. Tech. **27**, 140 (2016). https://doi.org/10.1007/s41365-016-0141-3
62. X.G. Deng, Y.G. Ma, M. Veselský, Thermal and transport properties in central heavy-ion reactions around a few hundred MeV/nucleon. Phys. Rev. C **94**, 044622 (2016). https://doi.org/10.1103/PhysRevC.94.044622